

2 copies.

1

SAND95-2215C

CONF-960774--1

150 11 2000

© S.T.

Shock Equation of State Properties of Concrete*

Dennis Grady

Experimental Impact Physics Department

Sandia National Laboratories

Albuquerque, New Mexico, 87185-5800, USA

Abstract

Unique shock compression experiments have been developed and pursued which provide material equation of state data for dynamic strength, pore crush, shock Hugoniot and adiabatic decompression. Experimental data have been obtained on an aggregate concrete to Hugoniot pressures of 25 GPa. New analytic methods were developed to extract equation-of-state properties from dynamic test data. Unexpected residual strain results are compared with expected thermal expansion and dilatancy properties of concrete.

1 Introduction

Experimental shock and adiabatic release data have been determined for concrete over a shock pressure range of approximately 3-25 GPa. In the experimental method a concrete sample (disc) is mounted in a projectile and undergoes planar impact on a thin disc of metal (copper or tantalum). Subsequent acceleration of the metal plate is monitored with diffused-surface velocity interferometry. A single measured acceleration history establishes both the initial shock compression Hugoniot state, and states on the decompression adiabat from that specific Hugoniot state.

Dynamic unloading properties of concrete are not well understood. Such properties are critical to the impact response of concrete because of the complex compaction and uncertain void volume in the cementitious component of the aggregate concrete. The experiments pursued in the present study offer a technique for measuring dynamic release properties of this complicated heterogeneous material. Previous applications of the impact-plate

* Sponsored by the U.S. Department of Energy and conducted under the auspices of the U. S. Department of Energy under Contract DE-AC04-94AL85000.

acceleration method have been reported by Rosenberg and Ahrens¹, Lysne et al.², and Chhabildas and Grady³.

2 Experimental Method

The shock compression and release experiments were performed on a single-stage 89-mm diameter smooth-bore powder gun capable of controlled impact velocities over 0.5-2.5 km/s. The reverse ballistics experimental configuration used to determine shock compression and release properties of concrete is illustrated in Figure 1. The concrete sample is mounted in the projectile as shown. A metal target or witness plate (disc) is mounted in a stationary target assembly and back-surface motion of the plate is measured by VISAR methods, e.g. Barker and Hollenbach⁴. In the present study both copper and tantalum were used as metal target plate material. Higher shock impedance of the tantalum results in higher Hugoniot pressures at a specified impact velocity. A table of pertinent experimental parameters for the present tests are provided in Table 1. The concrete material tested contained 3/8" quartz aggregate and had a density of 2260 kg/m³. Earlier dynamic material property data for the present concrete have been reported, e.g. Grady⁵.

3 Experimental Velocity Histories

Representative velocity histories measured with VISAR diagnostics are provided in Figures 2. Additional experiments performed with tantalum target plates achieved the highest Hugoniot pressures in the concrete. Although

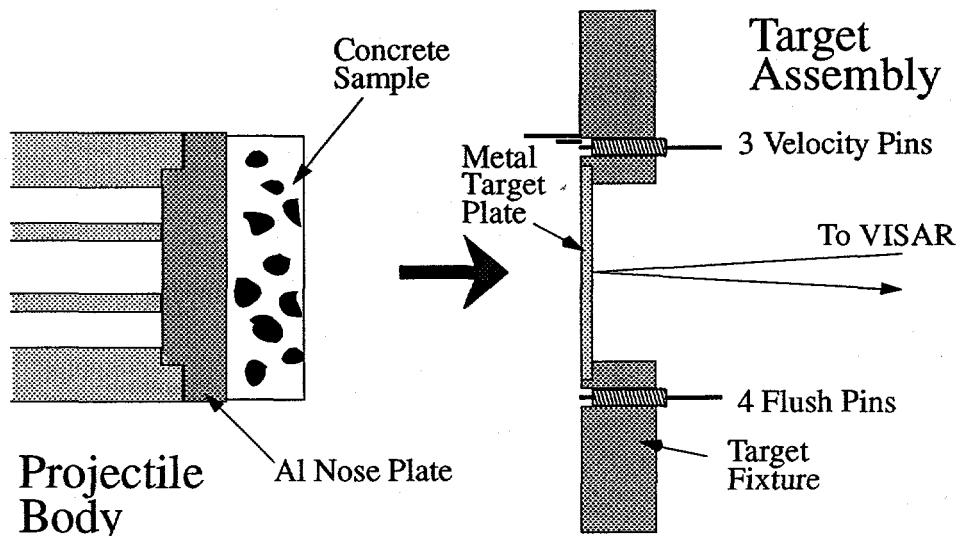


Figure 1: Experimental configuration for shock compression and release measurements on concrete.

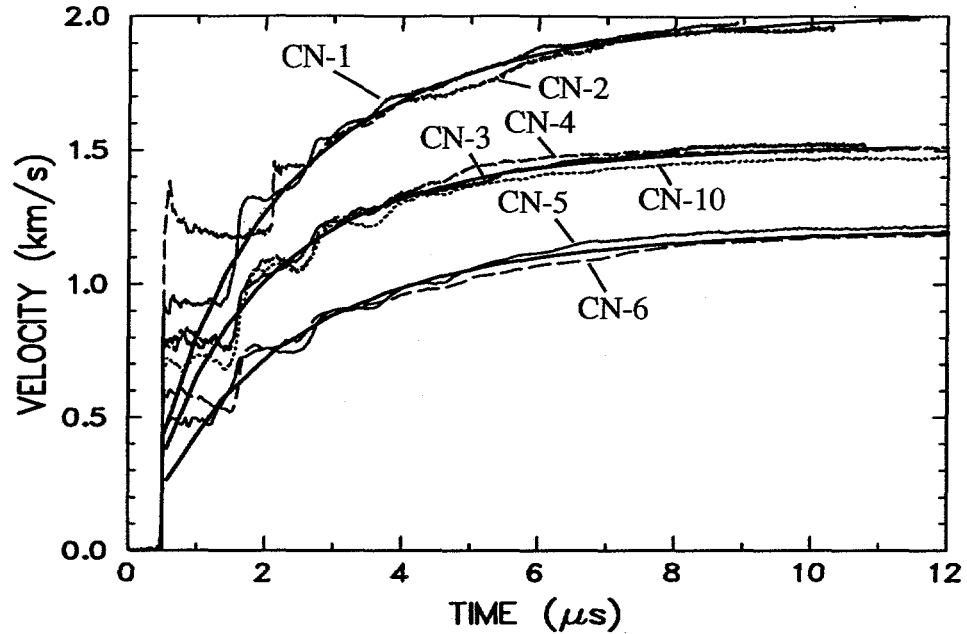


Figure 2: Velocity history data with copper witness plates. Solid curves are analytic fit (see text).

significant irregularities in the profiles are observed which are a consequence of the heterogeneous nature of the aggregate concrete, the initial plateau corresponding to the compressive shock state and the subsequent acceleration during decompression of the concrete sample are clearly observed.

Arrival of the second acceleration following the initial plateau in Figure 2 is consistent with expected wave velocity in the copper plate with the one exception of test CN-2. In this test it was concluded that aggregate and grout were configured in the concrete behind the VISAR diagnostic point in such a way as to produce a sharp pulse (as seen in the forward part of the first plateau) which locally spalled the copper. Delay in the second acceleration for this test is a consequence of time needed to reclose the spall gap. Consequently, the amplitude of the initial plateau is complicated by the spall behavior and this test was not used in the determination of a Hugoniot state.

4 Hugoniot Properties

Planar impact of the concrete sample on the stationary metal disc shocks both the concrete and the metal to their respective Hugoniot states. When the shock driven into the metal witness plate emerges at the back surface a reflected wave decompressing the metal to zero pressure is propagated back into the plate. The jump in velocity to a value of u_1 is determined by the amplitude of the shock and the release isentrope of the plate metal.

The pressure and particle velocity Hugoniot state (p_h and u_h) in the concrete are readily calculated from the measurement of u_1 and the equation of state properties of the witness plate metal,

$$u_h = V_p - u_m = V_p - \frac{u_1}{2}, \quad (1)$$

$$p_h = p_m = \rho_m C_m \frac{u_1}{2} + \rho_m S_m \left(\frac{u_1}{2} \right)^2. \quad (2)$$

In Equations 1 and 2 V_p is the projectile velocity while the set $\{\rho_m, C_m, S_m\}$ constitute the Hugoniot properties of the witness plate metal in a linear shock-velocity-versus-particle-velocity relation. Shock velocity and Hugoniot strain are not directly measured but can be calculated through the Hugoniot conservation relations. Hugoniot properties are provided in Table 1.

5 Release Properties

Subsequent acceleration of the witness plate following the first (Hugoniot state) plateau is governed by the dynamic decompression properties of the concrete from the Hugoniot state. These unique data reveal the release equation-of-state properties of the shock-compressed concrete over a wide range of pressures below the Hugoniot pressure. The data also reflects hysteretic properties occurring through void collapse and material strength. In the present study a continuous analytic method is pursued to determine the release equation-of-state paths of the test concrete. For times following initial shock compression of concrete and witness-plate metal, starting at emergence of the shock wave at the metal free surface (start of VISAR recorded motion), the witness plate is treated as a lumped mass (mass per unit area) accelerating under the time-dependent pressure at the concrete-metal interface. This approximation is acceptable when numerous wave reflections through the plate thickness occur over the time of interest.

The pressure-versus-particle-velocity release behavior of the concrete is determined through solution of the equation of motion governing acceleration of the metal witness plate. The corresponding pressure-versus-volume behavior is calculated through solution of the appropriate Riemann integral and is dependent on assumptions concerning the simple wave nature of the release wave following the compressive shock in the test concrete.

Assuming rigid motion of the metal witness plate, acceleration is governed by,

$$m\ddot{u} = p(u), \quad (3)$$

where $m = \rho_m h$, and where ρ_m and h are the metal density and plate thickness, respectively. To proceed, an analytic form will be assumed for the release pressure-versus-particle-velocity path of the concrete. A common representation for condensed matter in this space is a quadratic expression. This

arises, for example, from a linear shock-velocity-versus-particle-velocity relation for the pressure-particle velocity Hugoniot. The resulting functional form has also been found to represent well the hydrostatic compression of many solids — perhaps because of its close relationship to a Birch-Murnaghan equation of state, e.g. Jeanloz⁶. Consistent with the reference frame of the present experimental configuration, the expression,

$$p(u) = \rho_o S(u - u_f)^2 - \rho_o C(u - u_f), \quad (4)$$

will be assumed where the release path is reference from the final velocity u_f upon complete decompression. The initial material density is ρ_o while C and S are experimental fitting constants, although their close numerical similarity to the familiar shock-velocity-particle-velocity constants will be noted.

Introducing the change of variable $v = u - u_f$, Equations 3 and 4 have the particular solution,

$$\frac{v}{Sv - C} = \frac{v_o}{Sv_o - C} e^{-\frac{\rho_o S}{m} t}, \quad (5)$$

where $v_o = u_o - u_f$ with $p_o = p_m$ and $u_o = u_m$, the Hugoniot conditions in the witness plate metal, at $t = 0$.

From Equation 4 at the initial state, one obtains the solution,

$$v_o = \frac{C}{2S} \left(1 - \sqrt{1 + \frac{4Sp_o}{\rho_o C^2}} \right). \quad (6)$$

The initial pressure $p_o = p_m$ is known from the amplitude of the initial velocity step measured with the VISAR and the known Hugoniot properties of the metal. Equations 5 and 6 are used to calculate the velocity history of the witness plate corresponding to an initial velocity step u_1 and plate parameters ρ_m and h .

The parameters C and S in the pressure-versus-particle-velocity expression (Equation 4) are adjusted until the calculated velocity history provides an optimum agreement with the measured experimental acceleration profile. The resulting pressure-versus-particle-velocity path identifies the experimental release adiabat from the corresponding Hugoniot state. Optimum calculated velocity histories are shown with the copper witness plate experimental data in Figure 2. Nominally similar experiments exhibited a degree of scatter due to variability in concrete samples. Consequently, experiments were grouped as indicated on the right of Table 1. Values of C and S providing the best fit to the velocity data are given in Table 1.

The pressure-versus-volume release adiabat can be calculated from Equation 4 through the appropriate Riemann relations. Calculation of the strain $\epsilon = 1 - \rho_o / \rho$ assumes rate independent material response and simple wave behavior of the release wave following the initial compressive shock into the material. Simple wave behavior holds until the release wave overtakes the

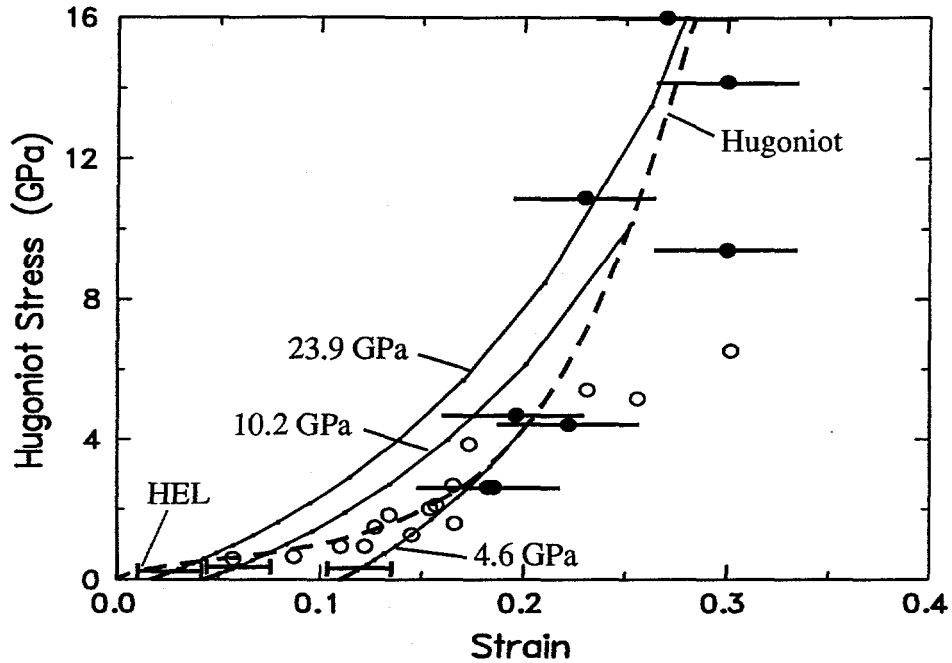


Figure 3: Release paths from 4.6, 10.2 and 23.9 GPa pressure states on the concrete Hugoniot. Scatter bars for the release paths are indicated near the lower portion of the paths.

shock wave and information propagates back to the recording interface. One obtains,

$$\varepsilon = \varepsilon_{res} + \frac{1}{2S} \ln \left(\frac{2S}{C} (u - u_{res}) + 1 \right), \quad (7)$$

where ε_{res} is the residual strain upon release to zero pressure. Equation 7 can be combined with Equation 4 to provide the pressure versus volume strain relation,

$$p = \frac{\rho_o C^2}{4S} (e^{4S(\varepsilon - \varepsilon_{res})} - 1). \quad (8)$$

Lastly, a measure of the compressibility at the Hugoniot state is provided by the release wave velocity,

$$c_h = \frac{\rho_o}{\rho_h} (S(u_h - u_{res}) + C). \quad (9)$$

Values of ε_{res} and c_h determined from the acceleration data are also provided in Table 1. Representative dynamic release paths from states on the principal Hugoniot are shown in Figure 3.

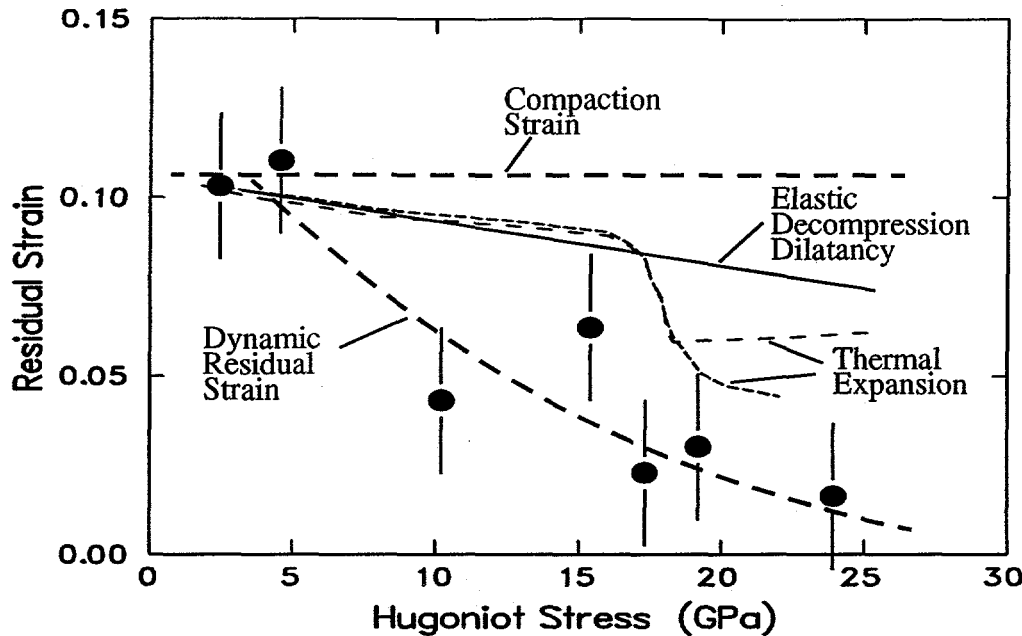


Figure 4: Residual strain data upon decompression from states on the concrete Hugoniot. A nominal quasistatic compaction strain for this concrete is also indicated. Calculated strain recovery due to shock-heating-induced thermal expansion (crystalline quartz and quartzite) and on elastic-anisotropy-induced expansion dilatancy are shown for comparison.

6 Discussion

Static and low pressure shock data indicate substantial volume compaction in the present concrete. Marked flattening of the Hugoniot immediately above the HEL (~0.5 GPa) before stiffening to a compressibility more characteristic of the solid rock component is common to the dynamic compaction of a porous material. Release paths from Hugoniot states in the range of 3-5 GPa indicate a 10-11% irrecoverable volume change consistent with compaction measurements under static loading.

Shock compression and release measurements to Hugoniot states in excess of 5 GPa and up to about 25 GPa indicate a decreasing irrecoverable volume strain. There are several possible explanations for this behavior.

One possibility is thermal expansion on shock recovery due to the extensive shock heating during the dynamic compaction event. Silica aggregate and sand in the concrete mixture constitute approximately 80% by weight of the material. Thus properties of quartz are appropriate in examining consequences of thermal expansion in the shock compression and release process.

Thermal expansion properties of crystalline quartz over the temperature range of concern are strongly nonlinear due primarily to the α - to β -quartz transformation occurring at approximately 550-600 C. Thermal expansion measurements, e.g. Dmitriev et.al.⁷, on single crystal α -quartz show a

maximum volume expansion of approximately 4.5% at about 580 C relative to room temperature (20 C) dimensions. Continued heating to 1000 C actually shows a slight reduction from the maximum. Measurements to 800 C on quartzite indicates a positive thermal expansion over the entire temperature range with a marked peak in the vicinity of the α - β transition.

Estimates of volume recovery due strictly to thermal expansion based on the above data, e.g. Dmitriev et.al.⁷, are shown in Figure 4. Residual shock temperature estimates are based on the assumption of uniform temperature through the material and calculated from the energy dissipated in a shock compression and release cycle. A value of $c_p = 800 \text{ J/kg/C}$ is appropriate for the specific heat of quartz, e.g. Dmitriev et.al.⁷.

Predictions based on thermal expansion due to shock heating can account for at best about half of the measured residual strain indicated by the data for concrete in Figure 4. Issues regarding the thermal expansion properties of the cement grout constituents and the heterogeneous nature of dissipation in the shock compression process should be examined further, however.

An additional mechanism for strain recovery during decompression from the shocked state can be traced to the elastic compliance of the material. Compaction and inelastic shear during the shock compression process eliminates all, or most, of the initial void volume, but leaves the material in a debonded, or weakly bonded, granular state at the Hugoniot pressure. The crystalline compliance of quartz (again we assume that quartz dominates the concrete shock mechanical response) is anisotropic. The trigonal crystal symmetry of quartz leads to a compliance with axial symmetry described by two material constants. In other words expansion of a crystallite during pressure release will be accompanied by a shape change as well as a solid volume change. Random orientation of grains in the material will lead to an incompatible bulk compliance during decompression and the opening of void volume. An estimate of the void volume can be made by considering a single anisotropic crystal in an otherwise isotropic matrix.

The anisotropic compliance of crystalline quartz can be reasonably characterized by two constants — the compliance β_{\parallel} parallel to the symmetry axis and the compliance β_{\perp} perpendicular to this axis. Values for quartz are $\beta_{\parallel} = 0.0067 \text{ GPa}^{-1}$ and $\beta_{\perp} = 0.0095 \text{ GPa}^{-1}$, e.g. Nye⁸.

Regarding as components of a second rank tensor the invariant $\beta_{\perp} + 2\beta_{\parallel}$ is responsible for the volume change whereas shape change is determined by the deviator expression $|\beta_{\perp} - \beta_{\parallel}|$. In a simple model of the dilatancy process during decompression it is shown that the ratio of dilatant void strain ϵ_d to the volumetric solid strain ϵ_s is given by,

$$\frac{\epsilon_d}{\epsilon_s} = \frac{\beta_{\perp} - \beta_{\parallel}}{\beta_{\perp} + 2\beta_{\parallel}}. \quad (10)$$

For quartz this ratio is about 11%. Based on this relation an estimate of the residual strain recovery due to the anisotropic compliance of quartz is compared with measurements in Figure 4.

Although neither thermal expansion or decompression dilatancy separately are sufficient to account for the observed residual strain recovery, taken together they are of the right order to perhaps explain the trend of the data.

The relatively large temperature rise in concrete corresponding to a few tens of GPa Hugoniot pressure is due primarily to the collapse of the 10-11% effective void in the material. Since approximately 80% by weight of the concrete is fully dense quartz this void is concentrated within the remaining 20% of the material — namely the cement grout component. Consequently, it is reasonable to speculate that release temperatures from Hugoniot states were not a modest homogeneous 600-800 C, but temperatures as much as five times these values concentrated in the cement grout might be expected.

Temperatures of this order would be expected to vaporize free water in the cement grout and probably volatilize a substantial portion of the hydrated materials. Volumetric expansion due to vaporization and volatilization on decompression from the shock state would appear to be a less likely explanation for the recovery strains observed in the present data, however. Examination of the release adiabats (see Figure 3) indicates that the observed recovery strains are accumulated over a substantial portion of the release. Expansion from vaporization and volatilization would be expected to occur over the last few tenths of a GPa as pressure approaches zero.

7 References

1. Rosenberg, J. T. & Ahrens, T. J. ASME Paper No. 66-WA/PT-7, Amer. Soc. Mech. Eng., New York, December, 1966.
2. Lysne, P. C., Boade R. R. , Percival C. M. & Jones O. E. Determination of Release Adiabats and Recentered Hugoniot Curves by Shock Reverberation Techniques, *J. Appl. Phys.*, 1969, **40**, 3786 (1969).
3. Chhabildas, L. C. & Grady, D. E. Dynamic Material Response of Quartz at High Strain Rates, *Mat. Res. Symp. Proc.*, pp 147-150, Elsevier, 1984.
4. Barker, L. M., & Hollenbach, R. E. Laser Interferometer for Measuring High Velocities of any Reflecting Surface, *J. Appl. Phys.*, 1972, **43**, 4669.
5. Grady, D. E., Impact Compression Properties of Concrete, *Proceedings of the Sixth International Symposium on Interaction of Nonnuclear Munitions with Structures*, Panama City Beach, Florida, 1993.
6. Jeanloz, R., Shock Wave Equation of State and Finite Strain Theory, *J. Geophys. Res.*, 1989, **94**, 5873.
7. Dmitriyev, A. P., Kuzyayev L. S., Protasov Yu. I., & Yamshchikov V. S. Physical Properties of Rocks at High Temperature, *NASA Technical Translation*, NASA TT F-684, June, 1972.
8. Nye, J. F., *Physical Properties of Crystals*, Oxford at the Clarendon Press, 1957.

Table 1:
Impact Experiment Parameters

Test Numb.	Density (kg/m ³)	Sample Thick. ² (mm)	Plate Mat 1.	Plate Thick. ³ (mm)	Impact Vel. (km/s)	u ₁ (km/s)	u _h (km/s)	p _h (GPa)	U _s (km/s)	ε _h	Test ⁴ Numb.	C (km/s)	S	ε _{res}	c _h (km/s)
JC23	2260	12.0	Cu	3.11	0.523	0.145	0.45	2.6	2.36	0.18	23,24	3.3	2.0	0.103	4.1
JC24 ¹	2290	12.0	Cu	3.18	0.524	0.145	0.45	2.6	2.32	0.18	25,26	3.7	2.2	0.110	5.2
JC25	2260	15.2	Cu	3.11	0.774	0.240	0.65	4.4	2.87	0.22	5,6	3.0	1.7	0.043	5.0
JC26 ¹	2290	15.0	Cu	3.14	0.775	0.255	0.65	4.7	3.06	0.20	3,4,10	4.1	2.0	0.063	6.6
CN1	2332	25.4	Cu	2.39	2.15	0.93	1.69	19.2	4.87	0.35	9	3.1	1.5	0.023	5.0
CN2	2325	25.3	Cu	2.36	2.14	—	—	—	—	—	1,2	3.0	1.5	0.030	5.4
CN3	2328	25.4	Cu	2.33	1.74	0.79	1.35	16.0	5.09	0.27	7,8	3.0	1.7	0.016	6.3
CN4	2327	25.3	Cu	2.39	1.71	0.80	1.31	16.2	5.31	0.25	1 Different concrete with similar density.				
CN5	2363	25.4	Cu	2.36	1.33	0.49	1.09	9.4	3.65	0.30	2 Sample diameter = 86 mm.				
CN6	2323	25.4	Cu	2.34	1.32	0.56	1.04	10.9	4.51	0.23	3 Plate diameter = 74 mm.				
CN7	2337	25.4	Ta	1.53	2.27	0.70	1.92	22.3	4.97	0.39	4 Nominally similar tests.				
CN8	2320	25.4	Ta	1.52	2.20	0.79	1.82	24.8	5.87	0.31					
CN9	2315	25.4	Cu	2.41	2.09	0.85	1.67	17.3	4.47	0.37					
CN10	2314	25.4	Cu	2.36	1.71	0.71	1.36	14.2	4.51	0.30					

DISCLAIMER

This report was prepared as an account of work sponsored by an agency of the United States Government. Neither the United States Government nor any agency thereof, nor any of their employees, makes any warranty, express or implied, or assumes any legal liability or responsibility for the accuracy, completeness, or usefulness of any information, apparatus, product, or process disclosed, or represents that its use would not infringe privately owned rights. Reference herein to any specific commercial product, process, or service by trade name, trademark, manufacturer, or otherwise does not necessarily constitute or imply its endorsement, recommendation, or favoring by the United States Government or any agency thereof. The views and opinions of authors expressed herein do not necessarily state or reflect those of the United States Government or any agency thereof.